technologies

MDPI

Communication

Comparison of Shallow (−20 °C) and Deep Cryogenic Treatment (−196 °C) to Enhance the Properties of a Mg/2wt.%CeO_2 Nanocomposite

Shwetabh Gupta †, Gururaj Parande and Manoj Gupta *

Department of Mechanical Engineering, National University of Singapore, 9 Engineering Drive 1, Singapore 117575, Singapore
* Correspondence: mpegm@nus.edu.sg; Tel.: +65-6516-6358
† Current address: Blackett Laboratory, Imperial College, London SW7 2AZ, UK.

Abstract: Magnesium and its composites have been used in various applications owing to their high specific strength properties and low density. However, the application is limited to room-temperature conditions owing to the lack of research available on the ability of magnesium alloys to perform in sub-zero conditions. The present study attempted, for the first time, the effects of two cryogenic temperatures (−20 °C/253 K and −196 °C/77 K) on the physical, thermal, and mechanical properties of a Mg/2wt.%CeO_2 nanocomposite. The materials were synthesized using the disintegrated melt deposition method followed by hot extrusion. The results revealed that the shallow cryogenically treated (refrigerated at −20 °C) samples display a reduction in porosity, lower ignition resistance, similar microhardness, compressive yield, and ultimate strength and failure strain when compared to deep cryogenically treated samples in liquid nitrogen at −196 °C. Although deep cryogenically treated samples showed an overall edge, the extent of the increase in properties may not be justified, as samples exposed at −20 °C display very similar mechanical properties, thus reducing the overall cost of the cryogenic process. The results were compared with the data available in the open literature, and the mechanisms behind the improvement of the properties were evaluated.

Keywords: magnesium; nanocomposite; cryogenic treatment; mechanical properties; grain size

Citation: Gupta, S.; Parande, G.; Gupta, M. Comparison of Shallow (−20 °C) and Deep Cryogenic Treatment (−196 °C) to Enhance the Properties of a Mg/2wt.%CeO_2 Nanocomposite. *Technologies* **2024**, *12*, 14. https://doi.org/10.3390/technologies12020014

Academic Editor: Francesco Tornabene

Received: 2 November 2023
Revised: 12 January 2024
Accepted: 21 January 2024
Published: 23 January 2024

1. Introduction

Cryogenic treatment for metals has been established for almost 300 years primarily for enhancing the resistance to wear and localized indentation in steels [1–5]. In most of the studies, liquid nitrogen is used as a cryogenic medium corresponding to a temperature of −196 °C. Another commonly used medium is dry ice (−84 °C/189 K) [5]. There has been no systematic research attempt made, and there is no such attempt available in the open literature that uses comparatively higher temperatures in the cryogenic domain to investigate the properties of materials.

In the context of the cryogenic treatment of metallic materials, researchers have investigated materials based on iron, aluminum, and magnesium [1–3]. Among these materials, magnesium-based materials are gaining prominence due to their lightweight (~33% lighter than aluminum-based materials) and nontoxic and nutritional characteristics [6–10]. These properties are currently sought after to mitigate global warming and the toxification of land and water bodies. Among magnesium-based materials, magnesium nanocomposites have emerged as highly promising materials. Numerous studies have demonstrated that incorporating nanoparticles into magnesium and its alloys can significantly enhance its thermal properties, static and dynamic responses, and machining and wear properties [2,8,11–18]. The literature review indicates that no prior work has so far been conducted to explore the effects of cryogenic treatment on the response of magnesium nanocomposites. Furthermore, no work has been completed to compare the effects of a shallow cryogenic treatment

(−20 °C in freezer) and a deep cryogenic treatment (−196 °C in liquid nitrogen) on the physical, thermal, and mechanical responses of magnesium nanocomposites.

Accordingly, the present study aims to address these research gaps by investigating the above for an Mg/2wt.%CeO_2 nanocomposite, highlighting the capability of shallow cryogenic treatment (−20 °C) as a cost-effective way to improve multiple properties of the magnesium nanocomposite.

2. Materials and Methods

2.1. Materials Processing

Raw materials such as monolithic magnesium turnings (99.9% purity; supplier: ACROS Organics, Waltham, MA, USA) and cerium oxide (CeO_2) nanoparticles (size 15–30 nm; supplier: Alfa Aesar, Ward Hill, MA, USA) were utilized to produce the composite through the disintegrated melt deposition (DMD) method [19]. The raw materials were arranged in a multilayer arrangement and heated to a superheating temperature of 750 °C. The materials were arranged in a graphite crucible, and argon was used as the protective gas. To ensure the homogenization of the temperature and a uniform distribution, the molten magnesium composite melt was stirred for 150 s using a mild steel impeller. Post stirring, the melt was bottom poured into a steel mold to obtain a solid ingot. The ingots were machined, soaked at 400 °C for 1 h, and hot extruded at 350 °C using an extrusion ratio of 20.25:1 to obtain cylindrical rods of 8 mm diameter. The sub-zero immersion time was chosen based on the recommendations made in the open literature [1,3]. The temperature used for the shallow cryogenic treatment (RF) was −20 °C, and the temperature for the deep cryogenic treatment (LN) was −196 °C on the extruded samples for 24 h, respectively.

2.2. Characterization

2.2.1. Density and Porosity

The experimental densities were calculated using Archimedes' principle. Five samples were measured using an A&D GH-252 electronic balance with a standard deviation of ±1 mg. The theoretical densities of Mg (1.738 g·cm^{-3}) and CeO_2 (7.132 g·cm^{-3}), respectively, were used for the theoretical density calculation of the nanocomposite using the rule of mixtures. Porosity values were computed by comparing the experimental and theoretical densities.

2.2.2. Microstructure

The grain size of the samples was analyzed using a JEOL JSM-6010 Scanning Electron Microscope (SEM) as per ASTM E112-13. The samples were prepared by grinding, polishing, and etching before SEM observation. Oxalic acid was used as the etchant.

X-ray diffraction (XRD) studies along the longitudinal direction were performed using the Shimadzu LAB-XRD-6000 automated spectrometer with Cu K_α radiation of 1.54 Å wavelength and a scan speed of 2 °min^{-1}.

2.2.3. Thermal Properties

A Shimadzu DSC-60 differential scanning calorimeter (DSC) was used to analyze the effect of the cryogenic treatments on the thermal response of the samples. An argon gas flow rate of 25 mL·min^{-1} with a heating rate of 5 °C min^{-1} and a temperature range of 30–600 °C was used.

Thermogravimetric analysis (TGA) was performed to ascertain the ignition temperatures of the samples. Purified air with a flow rate of 50 mL·min^{-1} and a heating rate of 10 °C min^{-1} within a temperature range of 30–1000 °C were used.

2.2.4. Mechanical Properties

The microhardness was measured on the cryogenically treated samples using a Shimadzu-HMV automatic digital microhardness tester with a Vickers indenter as per

ASTM standard E384-08. An indentation load of 245.2 mN with a dwell time of 15 s was used, and a minimum of 20 readings per sample were taken.

Quasi-static room-temperature compression testing was carried out using an MTS E44 fully automated servohydraulic mechanical testing machine at a strain rate set at 5×10^{-3} min^{-1}. A minimum of three samples with a length-to-diameter (L/D) ratio of 1 were tested.

A JEOL JSM-6010 Scanning Electron Microscope was used to analyze the post-fracture behavior.

3. Results and Discussion

3.1. Density and Porosity Measurements

The results of the density measurements and porosity are summarized in Table 1. The density increased and porosity reduced after both cryogenic treatments. The percentage reduction was ~10.4% after the cold treatment (RF samples) and ~44% in the case of the deep cryogenic treatment (LN samples).

Table 1. The density and porosity measurements of Mg/2wt.%CeO_2 nanocomposite before and after cryogenic treatments.

Material	Theoretical Density ($g \cdot cm^{-3}$)	Before CT		After CT		
		Experimental Density ($g \cdot cm^{-3}$)	Porosity (%)	Experimental Density ($g \cdot cm^{-3}$)	Porosity (%)	Change in Porosity (%)
Pure Mg [a]	1.7380	1.732 ± 0.0005	0.3190	–	–	
Mg-2CeO_2 (AE)	1.7648	1.745 ± 0.002	1.099	–	–	
Mg-2CeO_2 (RF)	1.7648	1.7454 ± 0.008	1.102	1.7474 ± 0.001	0.9875	↓10.4
Mg-2CeO_2 (LN)	1.7648	1.7476 ± 0.0009	0.9764	1.755 ± 0.002	0.5445	↓43.3

[a] Values generated in the laboratory using similar raw materials and processing methods [13]. Note: AE—As Extruded; AE + RF—As Extruded + Shallow Cryogenic Treatment; AE + LN—As Extruded + Liquid Nitrogen Treatment. Note: '↓' represents the decrease in porosity before and after cryogenic treatment.

The reduction in porosity can be attributed to the compressive stresses generated during the cryogenic treatments with lower temperatures, yielding more remarkable effects [1–3]. The reduction in porosity in both cases also suggests that, under both cryogenic treatments, the material is capable of deforming inward into free space provided by pores. Furthermore, the reduction in porosity can also be attributed to the ability of the pores to serve as sinks for the dislocations generated during the cryogenic treatments [1,20].

3.2. Microstructure

Two aspects of the microstructure were characterized: the grain size and texture. The results of the grain size measurements are shown in Table 2. The grain size analysis of the samples is shown in Figure 1. The average grain size increased (up to 45%) for both types of cryogenic treatments. The increase in grain size, while unexpected, can be attributed to the simultaneous effects of (a) the capabilities of grains to orient themselves during cryogenic treatments [21], (b) the influence of compressive stresses to create order at the grain boundary region, leading to the merger of small grains with big grains (Figure 2), and (c) the capability of the defects to migrate to the grain boundaries [1]. The results also revealed that the average aspect ratio decreased with a decrease in the cryogenic temperature from −20 °C to −196 °C.

Table 2. The grain size measurements of the samples.

Composition	Grain Size (μm)	Aspect Ratio
Pure Mg	21 ± 0.8	1.4 ± 0.2
Mg-2CeO_2 (AE)	2 ± 0.6	1.4 ± 0.3
Mg-2CeO_2 (RF)	2.9 ± 1.0	1.3 ± 0.2
Mg-2CeO_2 (LN)	2.8 ± 0.6	1.2 ± 0.3

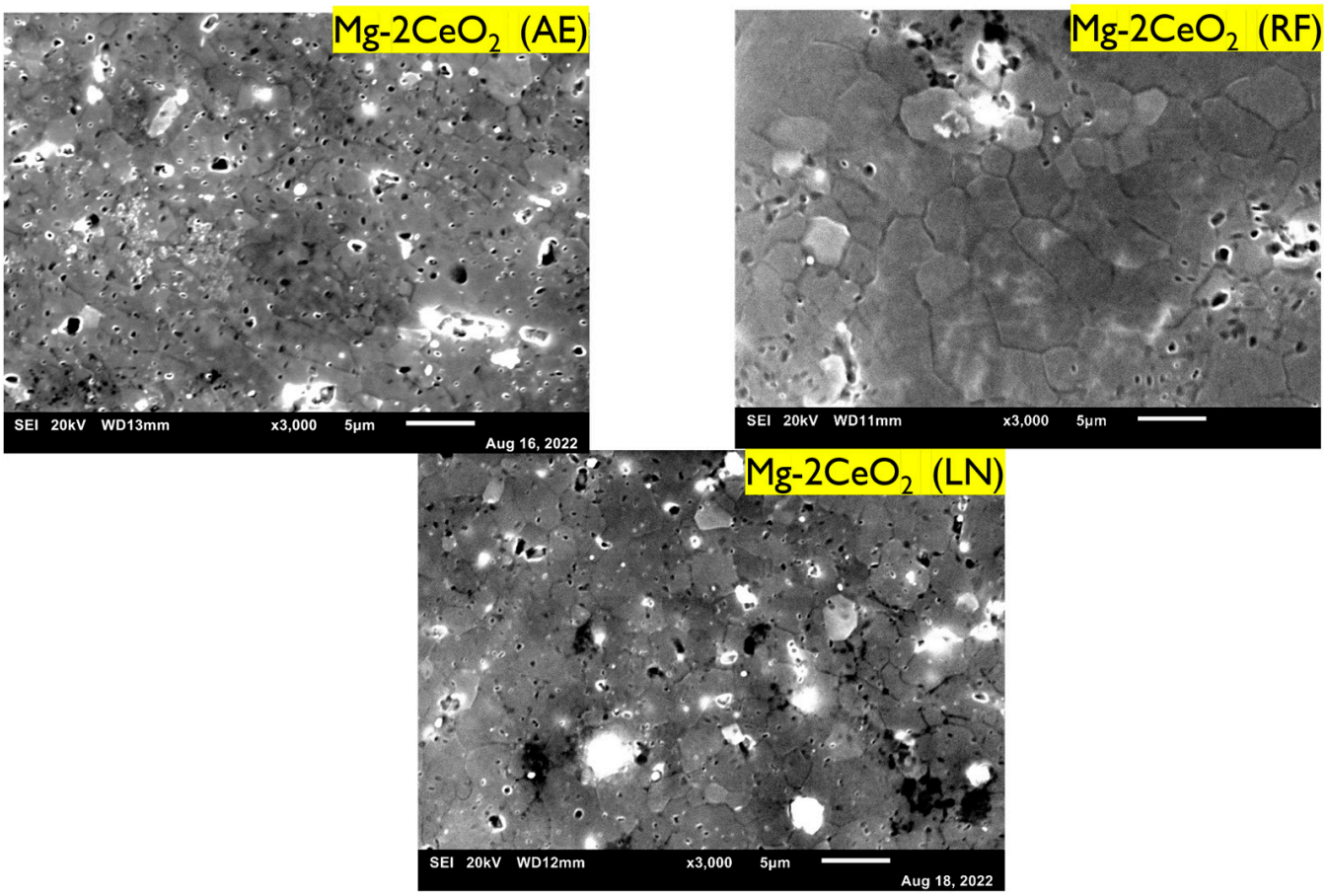

Figure 1. Microstructural characterization of the samples.

The results of the XRD studies indicated the dominance of the basal texture in the as-extruded (AE), cold-treated (RF), and DCT (LN) samples (Figure 3). However, the relative intensities (I/I_{max}) of the LN samples were higher compared to the RF samples, indicating that the RF samples have a stronger fiber texture when compared to the LN samples. The results thus suggest that variation in the cryogenic temperature leads to a variation in the degree of the microstructural evolution, which will have varying effects on the properties, provided that such a difference is substantial.

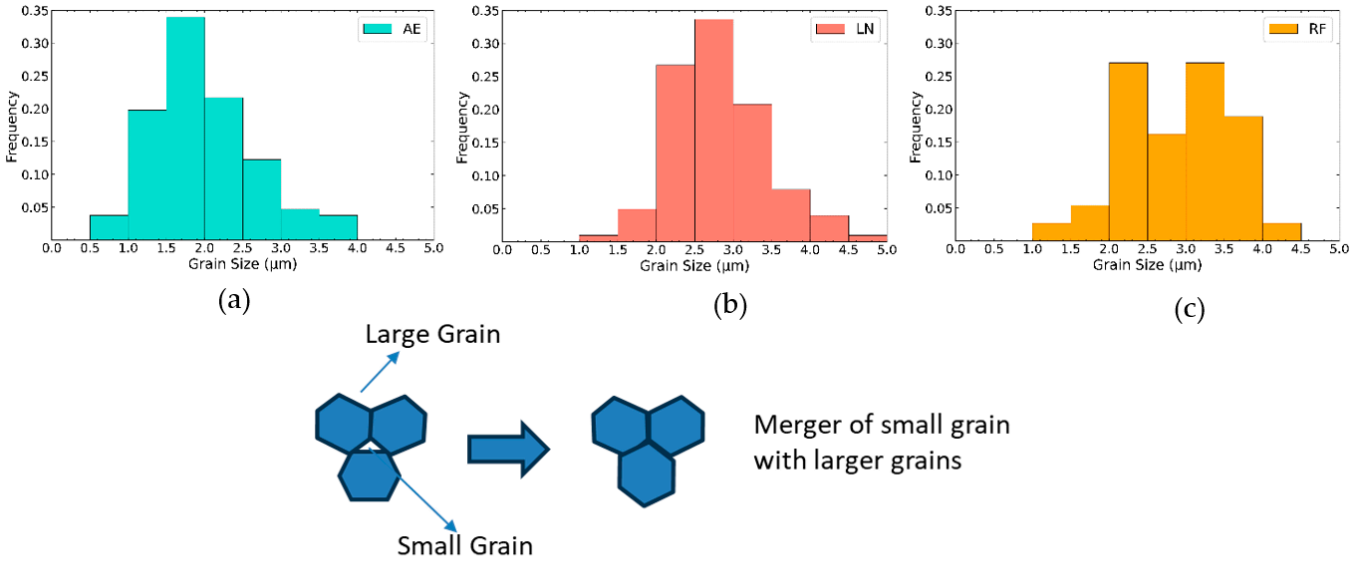

Figure 2. (**a**–**c**) Histograms of the frequency distributions of the various grain sizes within the Mg/2%wt. CeO_2 samples. It can be observed that the cryogenic treatment results in the frequency of grains smaller than 2 μm being significantly decreased along with an increase in the frequency of larger grains, indicating the merger of smaller grains and larger grains during the cryogenic treatments. (**d**) The proposed mechanism of the grain merger is shown.

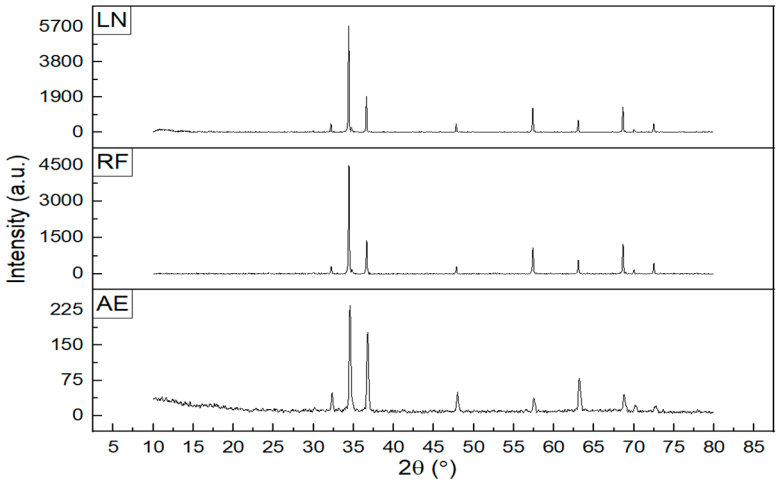

Material	Plane	I/I_{max}
Mg-2CeO_2 (AE)	10-10 prism	0.217021
	0002 basal	1
	10-11 pyramidal	0.753191
Mg-2CeO_2 (RF)	10-10 prism	0.071429
	0002 basal	1
	10-11 pyramidal	0.307966
Mg-2CeO_2 (LN)	10-10 prism	0.104399
	0002 basal	1
	10-11 pyramidal	0.52514

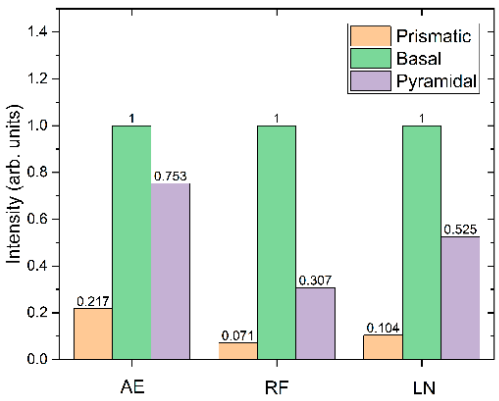

Figure 3. The results of the X-ray diffraction studies.

3.3. Thermal Response

The thermal response of the samples was evaluated in terms of the DSC studies (Figure 4) and the determination of the ignition temperature (Table 3). Visible peaks were observed at a temperature of ~470 °C and ~450 °C for the LN and RF samples, respectively. This observation was made in the author's past work on LN samples [22]. These findings suggest the release of stresses accumulated during the CT treatment in the case of the LN and RF samples. Further work is required in this area to understand this mechanism. It is worth noting that as the matrix is pure Mg, peaks due to dissolution or precipitation of other elements can be ruled out.

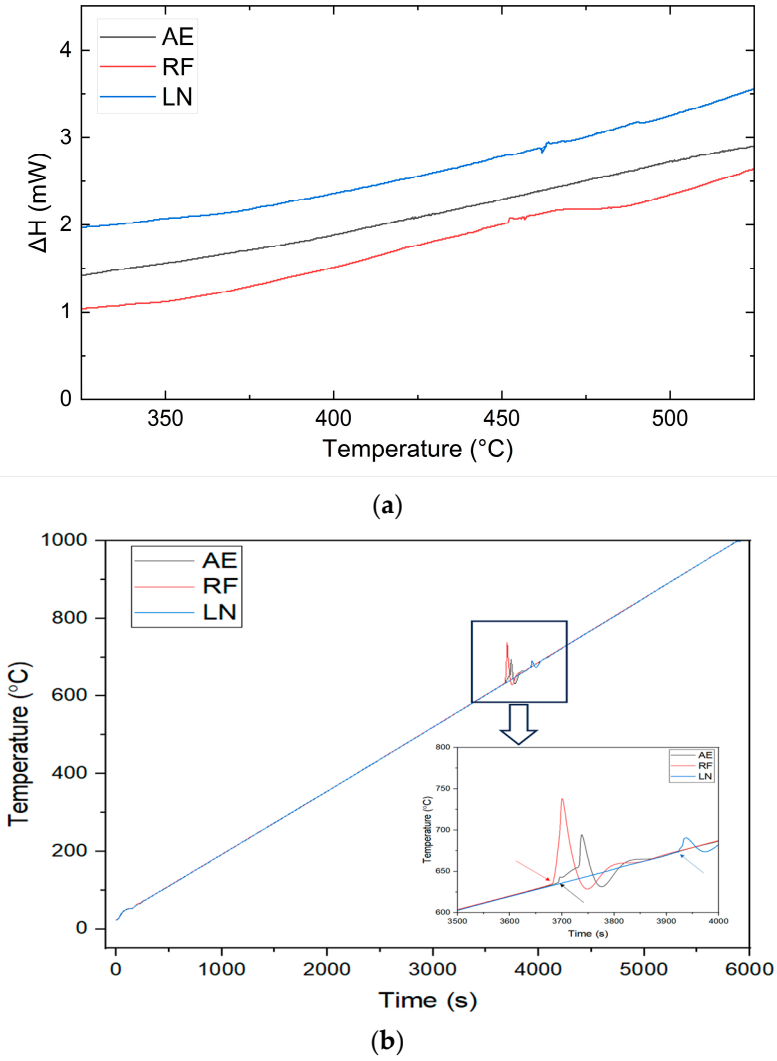

Figure 4. The results of the thermal analysis studies; (**a**) the DSC and (**b**) the ignition temperature of the samples.

The ignition temperature studies (Figure 4) indicated that the RF samples exhibited a similar ignition temperature, while the LN samples displayed a 38 °C increase compared to the as-extruded samples (Table 3). These results suggest that an increase in the ignition temperature in the LN samples can be attributed to an increase in the dislocation density during the LN treatment [22,23]. In contrast, the RF samples did not generate sufficient dislocations, thereby displaying no change in ignition characteristics.

It is noteworthy that the ignition temperatures of all the nanocomposite samples (AE, RF, and LN) remained superior to those of the commonly used commercial magnesium alloys (AZ and ZK series and WE 43 alloy), with the LN samples delivering the most favorable results.

Table 3. The ignition temperature measurements of the samples.

Composition	Ignition Temperature (°C)
Pure Mg	580
Mg-2CeO_2 (AE)	636
Mg-2CeO_2 (RF)	635 (↓1)
Mg-2CeO_2 (LN)	674 (↑38)
AZ31 [a]	628
AZ61 [a]	559
WE43 [a]	644
AZ91 [a]	600
ZK40A [a]	500
ZK60A [a]	499
AM50 [a]	585
AZ81A [a]	543

[a]—[24]. Note: (↑↓) changes are with respect to Mg-2CeO_2 (AE).

3.4. Mechanical Response

The mechanical response of the samples (AE, RF, and LN) was assessed in terms of the hardness (Table 4) and bulk compressive properties (Table 5).

Table 4. The microhardness measurements of the samples.

Composition/Treatment	Microhardness (HV)
Pure Mg	55 ± 3
Mg-2CeO_2 (AE)	74 ± 3
Mg-2CeO_2 (RF)	89 ± 5 (↑20%)
Mg-2CeO_2 (LN)	92 ± 4 (↑24%)

Note: (↑%) changes are with respect to Mg-2CeO_2 (AE).

Both the RF and LN samples exhibited superior hardness when compared to the AE samples. This can be attributed to the capability of the sub-zero temperature exposure's ability to (a) increase the dislocation density [1,20–22], (b) reduce porosity (Table 1), and (c) strain the lattice due to the induced compressive stresses [1,20,21]. All these factors increase the resistance to local deformation as experienced by the samples during hardness testing. Note that while the average microhardness of the RF samples remained marginally lower when compared to the LN samples, the difference is statistically insignificant, as their standard deviations overlap with each other.

The bulk compressive response of the AE, RF, and LN samples is interpreted each for 0.2 CYS, UCS, and failure strain. The 0.2 CYS of the RF and LN samples remained notably higher (up to 14% for LN samples) compared to the AE samples, indicating the capability of the sub-zero treatments to enhance the applicability of Mg nanocomposites for strength-based designs, which are typically based on yield strength. Between the RF and LN samples, the 0.2 CYS of the LN samples remained ~9% higher when compared to the RF samples. This increase in 0.2 CYS for the RF and LN samples indicates an increase in the stress required to initiate the motion of the unlocked dislocations [25]. This can primarily be attributed to the increase in the compressive stresses in the matrix rather than the grain size, as the grain size of both the RF and LN samples remained higher than the AE samples (Table 2). The results underscore the dominant role played by the induced compressive

stresses due to sub-zero treatments, mitigating the Hall–Petch softening in the case of the RF and LN samples.

The ultimate compressive strength (UCS) of both the RF and LN samples remained lower than the AE samples by a maximum of ~7% (RF samples). Between the RF and LN samples, the difference in the UCS can be considered insignificant given the overlap in standard deviations. The average UCS, however, remains higher for the LN samples by ~2.5% over the RF samples. These findings suggest the reduced work-hardening capability of the RF and LN samples. When computing Ds (difference in UCS and 0.2 CYS), the values were 299 MPa for AE, 255 MPa for RF, and 249 MPa for the LN samples. Both the RF and LN samples clearly exhibited lower work-hardening capabilities when compared to the AE samples, while the difference in work-hardening capabilities remained negligible and in favor of the RF samples.

Table 5. The compressive property measurements of the samples.

Composition/ Treatment	0.2 CYS (MPa)	UCS (MPa)	Fracture Strain (%)	Energy Absorbed (MJ/mm^3)
Pure Mg	63 ± 4	278 ± 5	24 ± 1	45
Mg-2CeO_2 (AE)	178 ± 19	473 ± 16	16.5 ± 0.7	44 ± 2
Mg-2CeO_2 (RF)	186 ± 17(↑5%)	441 ± 12(↓7%)	29.1 ± 1.0 (↑76%)	73 ± 4 (↑65%)
Mg-2CeO_2 (LN)	203 ± 5 (↑14%)	452 ± 15 (↓4%)	29.7 ± 1.2 (↑80%)	76 ± 6 (↑72%)
Mg-2Nd-4Zn [a]	242	502	8	NA
AM50	110	312	11.5	
AZ91D	130	300	12.4	
AZ31	NR	250	28	
Mg-5Zn/5BG	NR	112.8	NR	
WE43	261 ± 16	420 ± 13	16.3 ± 1.0	
WE43 + Apatite	229 ± 6	380.1 ± 9.0	11.7 ± 0.5	
ME21	87	260	25	
WE54	210	325	27	
ZK60	159	472	12.4	
Mg4Zn3Gd1Ca	260 ± 3	585 ± 18	12.6 ± 0.3	
Mg4Zn3Gd1Ca-ZnO	355 ± 5	703 ± 40	10.6 ± 0.3	

[a]—Cryogenic treatment in liquid nitrogen (−196 °C) for 1 day [26]. Note: (↑↓%) changes are with respect to Mg-2CeO_2 (AE).

The fracture strain of both the RF and LN samples showed a remarkable improvement by a maximum of ~80% (LN samples). Between the RF and LN samples, the difference in the fracture strain remained negligible (29.1 and 29.7, respectively). The results underscore the unique capability of sub-zero treatments in enhancing the fracture strain, demonstrating that exposure to −20 °C provides similar benefits as exposure to liquid nitrogen (−196 °C). The increase in the fracture strain of the sub-zero-treated samples (RF and LN samples) can be attributed to (a) the reduction in porosity (reduced crack initiation sites), (b) the enhanced matrix-reinforcement bonding (reduced crack initiation sites) [22], and (c) the reduced work hardening, leading to an increase in the uniform plastic deformation zone before the cracks initiated and catastrophically propagated (Figure 5). These results indicate that, following cryogenic treatment, dislocations can move easily and over long distances when compared to the non-treated samples.

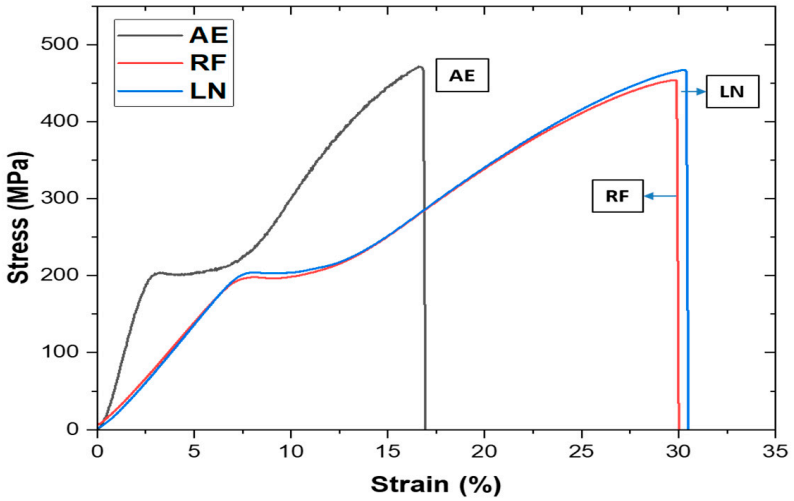

Figure 5. The compressive stress–strain diagrams for the AE, RF, and LN samples.

Fractographic studies conducted on the AE, RF, and LN samples are presented in Figures 6 and 7. Macrographs of all three samples show an approximately 45° fracture in relation to the compression axis. There was no remarkable difference between them visually.

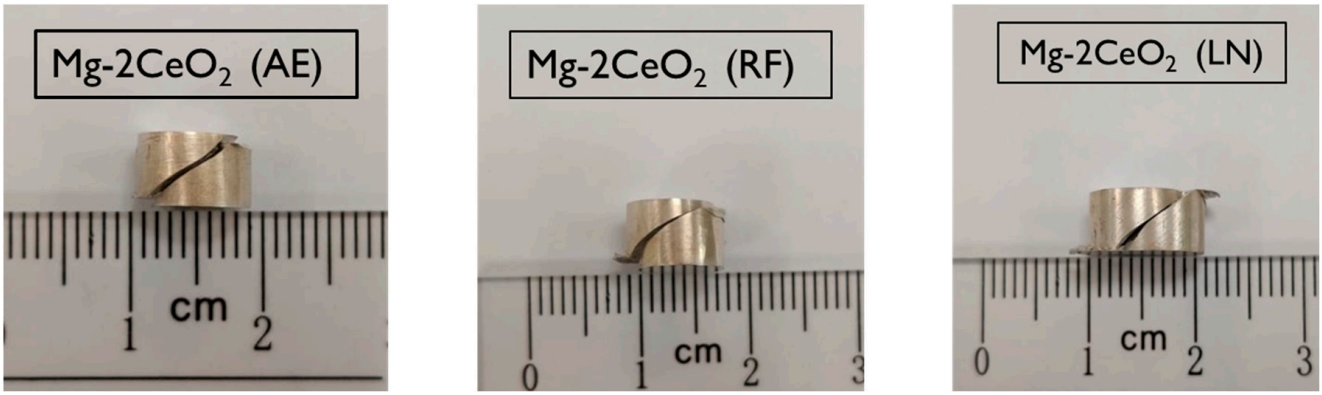

Figure 6. The macroscopic images of the compressively fractured samples.

Figure 7 presents the SEM micrographs of the fractured samples. A notable distinction is observed: the AE samples exhibit a relatively higher degree of flatness, indicative of a relatively brittle fracture, in contrast to the RF and LN samples, which exhibit a higher degree of roughness, signifying comparatively more plastic deformation.

The influence of deep cryogenic treatment on the elastic properties of magnesium materials depends on a complex interplay between dislocations and grain structure [27,28]. Dislocation pinning is promoted during cryogenic treatment, leading to an improvement in the elastic modulus. Furthermore, cryogenic treatment promotes the development of a preferred grain orientation (texture), resulting in the elastic properties becoming directionally dependent. Hence, specific textures might increase the elastic modulus in one direction but decrease it in another. Hence, while the overall trend often points toward an increased elastic modulus due to the grain refinement and dislocation pinning, the specific effects can vary greatly depending on the magnesium's material composition, microstructure, and treatment parameters. It is noteworthy that these effects will be different for nanocomposites, that no information in the open literature is available at this stage, and that systematic studies are required to isolate these effects for nanocomposites.

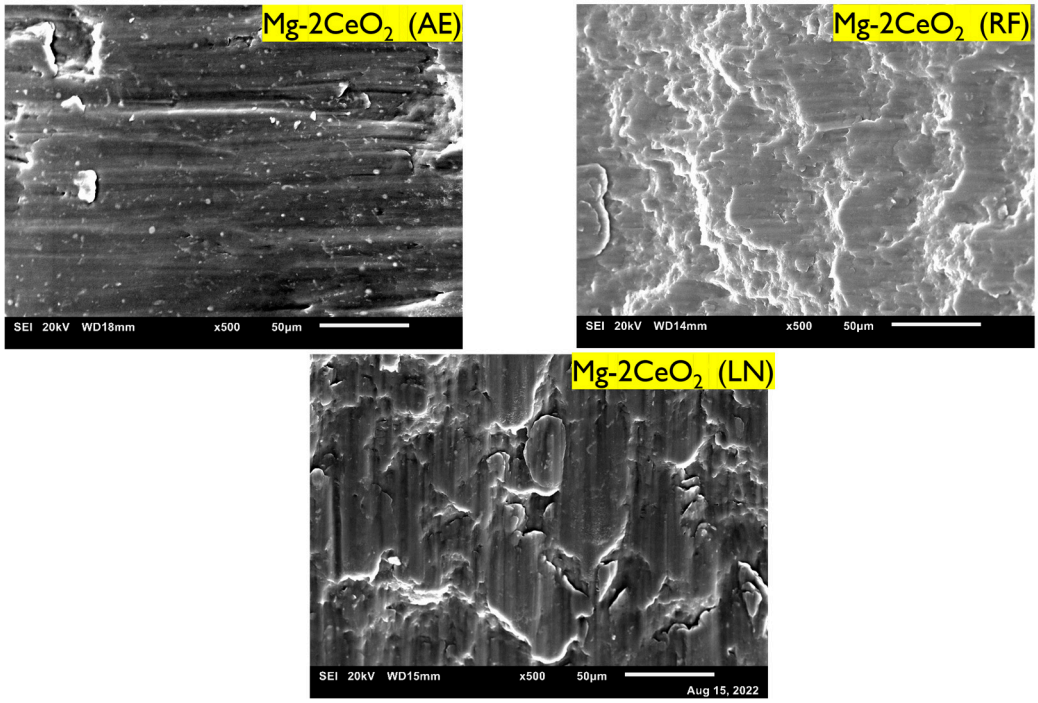

Figure 7. SEM images of the compressively fractured samples.

4. Conclusions

a. The porosity reduction of ~10.4% and ~43.3% was observed when compared with the AE samples when the samples were exposed to −20 °C (RF) and −196 °C (LN), respectively.
b. The DSC studies revealed the release of residual stresses in the case of the LN samples but not for the AE and RF samples.
c. The ignition temperature of the LN samples improved by 38 °C but decreased by only 1 °C for the RF samples when compared to the AE samples.
d. When exposed to shallow cryogenic treatment (−20 °C), the Mg-2CeO_2 nanocomposite showed a ~5%, ~76%, and ~65% increment in the 0.2 CYS, fracture strain, and energy absorption values, respectively, as compared to the untreated samples. By comparison, when exposed to deep cryogenic treatment (−196 °C), the Mg-2CeO_2 nanocomposite showed a ~14%, ~80%, and ~72% increment in the 0.2 CYS, fracture strain, and energy absorption values, respectively, as compared to the untreated samples. Overall, the UCS values for both conditions were slightly lower than the untreated conditions.
e. The fracture surfaces of the AE, RF, and LN samples did not reveal any noticeable difference at the visual level (45 ° shear fracture). The RF and LN samples showed a higher degree of surface roughness, indicating a higher fracture strain when compared to the AE samples.
f. The future outlook for the expansion of this field of research will be to focus in depth on the mechanism behind the improvement of the properties in a cryogenic setting and to identify suitable lightweight magnesium materials that can be suitable for such applications and to engineer them for high cryogenic performance.

Author Contributions: S.G.: Conceptualization, Methodology, Software, Formal analysis, Investigation, Data Curation, Writing—Original Draft, Writing Review and Editing, Visualization. G.P.: Formal analysis, Investigation, Data Curation, Writing—Review and Editing. M.G.: Conceptualization, Methodology, Writing—Review and Editing, Supervision, Project administration, Funding acquisition. All authors have read and agreed to the published version of the manuscript.

Funding: This research received no external funding.

Institutional Review Board Statement: Not applicable.

Informed Consent Statement: Not applicable.

Data Availability Statement: The data presented in this study are available on request from the corresponding author. The data are not publicly available due to confidentiality of research in some aspects.

Acknowledgments: The authors would like to thank the experimental support extended by Khin Sandar Tun and Hong Wei from the Department of Mechanical Engineering, National University of Singapore.

Conflicts of Interest: The authors declare that they have no known competing financial interests or personal relationships that could appear to have influenced the work reported in this paper.

References

1. Sonar, T.; Lomte, S.; Gogte, C. Cryogenic Treatment of Metal—A Review. *Mater. Today Proc.* **2018**, *5 Pt 3*, 25219–25228. [CrossRef]
2. Dieringa, H. Influence of Cryogenic Temperatures on the Microstructure and Mechanical Properties of Magnesium Alloys: A Review. *Metals* **2017**, *7*, 38. [CrossRef]
3. Baldissera, P.; Delprete, C. Deep cryogenic treatment: A bibliographic review. *Open Mech. Eng. J.* **2008**, *2*, 1–11. [CrossRef]
4. Das, D.; Ray, K.K.; Dutta, A.K. Influence of temperature of sub-zero treatments on the wear behaviour of die steel. *Wear* **2009**, *267*, 1361–1370. [CrossRef]
5. Barron, R.F. Cryogenic treatment of metals to improve wear resistance. *Cryogenics* **1982**, *22*, 409–413. [CrossRef]
6. Prasad, S.V.S.; Prasad, S.B.; Verma, K.; Mishra, R.K.; Kumar, V.; Singh, S. The role and significance of Magnesium in modern day research-A review. *J. Magnes. Alloys* **2022**, *10*, 1–61. [CrossRef]
7. Liu, L.; Chen, X.; Pan, F. A review on electromagnetic shielding magnesium alloys. *J. Magnes. Alloys* **2021**, *9*, 1906–1921. [CrossRef]
8. Shang, Y.; Pistidda, C.; Gizer, G.; Klassen, T.; Dornheim, M. Mg-based materials for hydrogen storage. *J. Magnes. Alloys* **2021**, *9*, 1837–1860. [CrossRef]
9. Staiger, M.P.; Pietak, A.M.; Huadmai, J.; Dias, G. Magnesium and its alloys as orthopedic biomaterials: A review. *Biomaterials* **2006**, *27*, 1728–1734. [CrossRef]
10. Kujur, M.S.; Manakari, V.; Parande, G.; Prasadh, S.; Wong, R.; Mallick, A.; Gupta, M. Effect of samarium oxide nanoparticles on degradation and invitro biocompatibility of magnesium. *Mater. Today Commun.* **2021**, *26*, 102171. [CrossRef]
11. Teo, Z.M.B.; Parande, G.; Manakari, V.; Gupta, M. Using low-temperature sinterless powder method to develop exceptionally high amount of zinc containing Mg–Zn–Ca alloy and Mg–Zn–Ca/SiO_2 nanocomposite. *J. Alloys Compd.* **2021**, *853*, 156957. [CrossRef]
12. Bupesh Raja, V.K.; Parande, G.; Kannan, S.; Sonawwanay, P.D.; Selvarani, V.; Ramasubramanian, S.; Ramachandran, D.; Jeremiah, A.; Akash Sundaraeswar, K.; Satheeshwaran, S.; et al. Influence of Laser Treatment Medium on the Surface Topography Characteristics of Laser Surface-Modified Resorbable Mg3Zn Alloy and Mg3Zn1HA Nanocomposite. *Metals* **2023**, *13*, 850. [CrossRef]
13. Parande, G.; Tun, K.S.; Neo, H.J.N.; Gupta, M. An Investigation into the Effect of Length Scale (Nano to Micron) of Cerium Oxide Particles on the Mechanical and Flammability Response of Magnesium. *J. Mater. Eng. Perform.* **2022**, *32*, 2710–2722. [CrossRef]
14. Wei, J.; He, C.; Qie, M.; Li, Y.; Tian, N.; Qin, G.; Zuo, L. Achieving high performance of wire arc additive manufactured Mg–Y–Nd alloy assisted by interlayer friction stir processing. *J. Mater. Process. Technol.* **2023**, *311*, 117809. [CrossRef]
15. Lopes, V.; Puga, H.; Gomes, I.V.; Peixinho, N.; Teixeira, J.C.; Barbosa, J. Magnesium stents manufacturing: Experimental application of a novel hybrid thin-walled investment casting approach. *J. Mater. Process. Technol.* **2022**, *299*, 117339. [CrossRef]
16. Yu, Z.; Chen, J.; Yan, H.; Xia, W.; Su, B.; Gong, X.; Guo, H. Degradation, stress corrosion cracking behavior and cytocompatibility of high strain rate rolled Mg-Zn-Sr alloys. *Mater. Lett.* **2020**, *260*, 126920. [CrossRef]
17. Maier, P.; Hort, N. *Magnesium Alloys for Biomedical Applications*; MDPI: Basel, Switzerland, 2020; Volume 10, p. 1328.
18. Joost, W.J.; Krajewski, P.E. Towards magnesium alloys for high-volume automotive applications. *Scr. Mater.* **2017**, *128*, 107–112. [CrossRef]
19. Prasadh, S.; Manakari, V.; Parande, G.; Wong, R.C.W.; Gupta, M. Hollow silica reinforced magnesium nanocomposites with enhanced mechanical and biological properties with computational modeling analysis for mandibular reconstruction. *Int. J. Oral Sci.* **2020**, *12*, 31. [CrossRef]
20. Huang, H.; Zhang, J. Microstructure and mechanical properties of AZ31 magnesium alloy processed by multi-directional forging at different temperatures. *Mater. Sci. Eng. A* **2016**, *674*, 52–58. [CrossRef]
21. Jiang, Y.; Chen, D.; Chen, Z.; Liu, J. Effect of Cryogenic Treatment on the Microstructure and Mechanical Properties of AZ31 Magnesium Alloy. *Mater. Manuf. Process.* **2010**, *25*, 837–841. [CrossRef]
22. Gupta, S.; Parande, G.; Tun, K.S.; Gupta, M. Enhancing the Physical, Thermal, and Mechanical Responses of a Mg/2wt.% CeO_2 Nanocomposite Using Deep Cryogenic Treatment. *Metals* **2023**, *13*, 660. [CrossRef]
23. Kogure, Y.; Hiki, Y. Effect of dislocations on low-temperature thermal conductivity and specific heat of copper-aluminum alloy crystals. *J. Phys. Soc. Jpn.* **1975**, *39*, 698–707. [CrossRef]

24. Tekumalla, S.; Gupta, M. An insight into ignition factors and mechanisms of magnesium based materials: A review. *Mater. Des.* **2017**, *113*, 84–98. [CrossRef]
25. Dieter, G.E.; Bacon, D. *Mechanical Metallurgy*; McGraw-Hill New York: New York, NY, USA, 1976; Volume 3.
26. Dong, N.; Sun, L.; Ma, H.; Jin, P. Effects of cryogenic treatment on microstructures and mechanical properties of Mg-2Nd-4Zn alloy. *Mater. Lett.* **2021**, *305*, 130699. [CrossRef]
27. Wang, J.; Xie, J.; Ma, D.; Mao, Z.; Liang, T.; Ying, P.; Wang, A.; Wang, W. Effect of deep cryogenic treatment on the microstructure and mechanical properties of Al–Cu–Mg–Ag alloy. *J. Mater. Res. Technol.* **2023**, *25*, 6880–6885. [CrossRef]
28. Jia, J.; Meng, M.; Zhang, Z.; Yang, X.; Lei, G.; Zhang, H. Effect of deep cryogenic treatment on the microstructure and tensile property of Mg-9Gd-4Y–2Zn-0.5Zr alloy. *J. Mater. Res. Technol.* **2022**, *16*, 74–87. [CrossRef]